Systems/Circuits

Functional Organization of Vestibulo-Ocular Responses in Abducens Motoneurons

Haike Dietrich,[1,2] **Stefan Glasauer,**[3] **and Hans Straka**[1]

[1]Department of Biology II and [2]Graduate School of Systemic Neurosciences, Ludwig-Maximilians-University Munich, 82152 Planegg, Germany, and [3]Center for Sensorimotor Research, Ludwig-Maximilians-University, 81377 Munich, Germany

Vestibulo-ocular reflexes (VORs) are the dominating contributors to gaze stabilization in all vertebrates. During horizontal head movements, abducens motoneurons form the final element of the reflex arc that integrates visuovestibular inputs into temporally precise motor commands for the lateral rectus eye muscle. Here, we studied a possible differentiation of abducens motoneurons into subtypes by evaluating their morphology, discharge properties, and synaptic pharmacology in semi-intact *in vitro* preparations of larval *Xenopus laevis*. Extracellular nerve recordings during sinusoidal head motion revealed a continuum of resting rates and activation thresholds during vestibular stimulation. Differences in the sensitivity to changing stimulus frequencies and velocities allowed subdividing abducens motoneurons into two subgroups, one encoding the frequency and velocity of head motion (Group I), and the other precisely encoding angular velocity independent of stimulus frequency (Group II). Computational modeling indicated that Group II motoneurons are the major contributor to actual eye movements over the tested stimulus range. The segregation into two functional subgroups coincides with a differential activation of glutamate receptor subtypes. Vestibular excitatory inputs in Group I motoneurons are mediated predominantly by NMDA receptors and to a lesser extent by AMPA receptors, whereas an AMPA receptor-mediated excitation prevails in Group II motoneurons. Furthermore, glycinergic ipsilateral vestibular inhibitory inputs are activated during the horizontal VOR, whereas the tonic GABAergic inhibition is presumably of extravestibular origin. These findings support the presence of physiologically and pharmacologically distinct functional subgroups of extraocular motoneurons that act in concert to mediate the large dynamic range of extraocular motor commands during gaze stabilization.

Key words: extraocular motoneurons; GABA; glutamate; glycine; semicircular canal; vestibulo-ocular reflex

Significance Statement

Outward-directed gaze-stabilizing eye movements are commanded by abducens motoneurons that combine different sensory inputs including signals from the vestibular system about ongoing head movements (vestibulo-ocular reflex). Using an amphibian model, this study investigates whether different types of abducens motoneurons exist that become active during different types of eye movements. The outcome of this study demonstrates the presence of specific motoneuronal populations with pharmacological profiles that match their response dynamics. The evolutionary conservation of the vestibulo-ocular circuitry makes it likely that a similar motoneuronal organization is also implemented in other vertebrates. Accordingly, the physiological and pharmacological understanding of specific motoneuronal contributions to eye movements might help in designing drug therapies for human eye movement dysfunctions such as abducens nerve palsy.

Introduction

Accurate perception of the visual environment in all vertebrates requires permanently active gaze stabilization that counteracts retinal image displacements during passive and self-motion. These image-stabilizing eye movements derive from the spatiotemporally precise transformation of visuovestibular sensory signals into extraocular motor commands. The large bandwidth of natural motion-related sensory signals likely precludes a signaling pathway composed of dynamically uniform neurons, but rather suggests that the underlying sensory-motor transforma-

Received Aug. 19, 2016; revised Feb. 7, 2017; accepted Feb. 9, 2017.

Author contributions: H.D., S.G., and H.S. designed research; H.D. and S.G. performed research; H.D. and S.G. analyzed data; H.D., S.G., and H.S. wrote the paper.

This work was supported by the German Science Foundation (Grants CRC 870, STR 478/3-1, and GL 342/2-1), the German Federal Ministry of Education and Research (Grant 01 EO 0901), and the Munich Center for Neurosciences–Brain and Mind (MCN). We thank Tobias Kohl for help with the spike 2 software scripts for the spike-sorting algorithm and Alexander Knorr for help with the eye motion analysis software.

The authors declare no competing financial interests.

Correspondence should be addressed to Dr. Hans Straka, Department of Biology II, Ludwig-Maximilians-University Munich, Großhaderner Str. 2, 82152 Planegg, Germany. E-mail: straka@lmu.de.

DOI:10.1523/JNEUROSCI.2626-16.2017

 0270-6474/17/374032-14$15.00/0

tion occurs in separate, parallel signaling channels with different temporal characteristics (see Straka and Dieringer, 2004; Straka et al., 2009). The necessity of such an organization is particularly obvious for the vestibulo-ocular reflex (VOR) pathway given the wide dynamic range of this system for motion encoding. Whereas both vestibular nerve afferents (Goldberg, 2000; Jamali et al., 2013) and central vestibular neurons (Straka et al., 2005) subdivide into distinct cellular subtypes, a similarly clear differentiation of extraocular motoneurons into functional phenotypes has so far not been demonstrated. Except for a few studies emphasizing potential differences in motoneuronal response patterns during head motion (Dieringer and Precht, 1986; Evinger and Baker, 1991; Davis-López de Carrizosa et al., 2011), distinct subgroups with respect to intrinsic membrane properties have thus far only been described for rat oculomotor motoneurons (Nieto-Gonzalez et al., 2007). Nonetheless, vertebrate extraocular motor nuclei appear to form morpho-physiologically heterogeneous populations of neurons with different recruitment thresholds and time constants that match the large behavioral spectrum of eye movements (Sterling, 1977; Delgado-Garcia et al., 1986; Pastor et al., 1991; Pastor and Gonzales-Forero, 2003; Carrascal et al., 2009; Davis-López de Carrizosa et al., 2011).

Functionally distinct subpopulations can also be observed at the level of extraocular muscle fibers that distinguish into tonic, multiply, and twitch-like, singly innervated fibers (Büttner-Ennever et al., 2001; Eberhorn et al., 2005, 2006). Assuming different contraction dynamics of the respective fiber types, this structural differentiation is excellently suited to meet the general necessity for eye muscles to cover different motion dynamics such as during saccades, smooth pursuit, gaze holding, or slow-phase optokinetic responses (Horn and Leigh, 2011). This differential neuromuscular innervation of two separate muscle fiber types suggests a bipartite organization of extraocular motoneurons (Büttner-Ennever et al., 2001; Ugolini et al., 2006). Moreover, to generate dynamically appropriate extraocular motor commands for different eye motion tasks, extraocular motoneurons require functionally adequate synaptic inputs (Dean, 1997). In fact, different types of extraocular motoneurons receive synaptic inputs from spatially segregated ocular motor control regions with complementary functions such as gaze stabilization or voluntary movement control during saccades or smooth pursuit (Ugolini et al., 2006).

Here, we provide direct evidence that extraocular motoneurons indeed form subgroups that mediate signals with distinct dynamics. During sinusoidal motion stimulation, abducens nerve recordings in semi-intact preparations of *Xenopus laevis* tadpoles revealed two groups of extraocular motor units that either modulated exclusively with head motion velocity or with both velocity and frequency components of the head movement. Pharmacological blockade of excitatory and inhibitory transmission demonstrated a differential impact of specific neurotransmitter systems and/or receptor subtypes for shaping the motor output of the two motoneuronal subgroups. Computational modeling that linked motor unit discharge with actual eye motion dynamics outlined potential contributions of the different neuronal subtypes to VOR performance. Preliminary data were previously published in abstract form (Dietrich et al., 2014).

Materials and Methods

Animals and experimental preparation. X. laevis tadpoles of either sex ($n = 122$) at developmental stages 53–54 (Nieuwkoop and Faber, 1994) were obtained from the in house animal breeding facility at the Biocenter-Martinsried (Ludwig-Maximilians-University Munich). As in previous studies (Chagnaud et al., 2015; Dietrich and Straka, 2016; Gensberger et al., 2016), animals at these developmental stages display the most robust eye movements between the functional onset of the horizontal VOR around stage 48/49 (Lambert et al., 2008) and the notable reduction in eye movement dynamics that occurs during metamorphic climax and subsequently in adult frogs (Straka and Simmers, 2012). Tadpoles were maintained in tanks with nonchlorinated water (17–18°C) at a 12/12 light/dark cycle and were fed daily with *Spirulina* bacteria. Electrophysiological and pharmacological experiments were performed *in vitro* on isolated, semi-intact preparations and comply with the National Institutes of Health's "Principles of Animal Care" (Publication No. 86-23, Revised 1985). Permission for these experiments was granted by the respective governmental institution at the Regierung von Oberbayern (55.2-1-54-2532.3-59-12).

For all experiments, tadpoles were anesthetized in 0.05% 3-aminobenzoic acid ethyl ester methanesulfonate (MS-222; Pharmaq) in ice-cold frog Ringer's solution containing the following (in mM): 75 NaCl, 25 $NaHCO_3$, 2 $CaCl_2$, 2 KCl, 0.5 $MgCl_2$, and 11 glucose, pH 7.4, and decapitated at the level of the upper spinal cord. As described previously (Gensberger et al., 2016), the skin above the brain was removed, the cartilaginous skull opened from dorsal, the forebrain and spinal cord disconnected, and both optic nerves transected. This excluded an influence of spinal locomotor efference copies (Lambert et al., 2012) and visual motion stimuli that theoretically would have been coactivated along with vestibular-driven eye movements and thereby confounded a classification according to head motion dynamics. The remaining CNS and vestibular sensory periphery, as well as all afferent connections and extraocular motoneuronal projections, were functionally preserved in this preparation. This allowed a natural activation of the horizontal VOR with sinusoidal vertical-axis rotations on a two-axis turntable under controlled *in vitro* conditions (Dietrich and Straka, 2016). Extraocular motor units were recorded from the abducens nerve after isolation of the lateral rectus (LR) nerve branch by cutting the nerve close to the target muscle innervation site with fine scissors. For pharmacological experiments, the trochlear nerve was isolated from the superior oblique (SO) muscle and used for control recordings. For anatomical tracer application, nerve branches were similarly prepared and cleaned from surrounding tissue. For all experiments, the preparations were placed in a Sylgard-lined recording chamber that was continuously perfused with oxygenated Ringer's solution at a constant temperature of 16.8 ± 0.1°C.

Electrophysiology and pharmacology. The recording chamber with the preparation affixed to the Sylgard floor was mounted in the center of the rotation axes of a two-axis computer-controlled motorized turntable (ACT-1002; Acutronic) as described previously (Lambert et al., 2008). Spontaneous and stimulus-evoked spike discharge of the abducens and trochlear nerves were recorded extracellularly (EXT 10-2F; NPI Electronics) with individually adjusted glass suction electrodes, digitized at 20 kHz (CED 1401; Cambridge Electronic Design), and stored on a computer for offline analysis. Glass suction electrodes were made from borosilicate glass (GB150-8P; 0.86 × 1.5 mm: inner and outer diameter, respectively; Science Products), which were pulled on a P-87 Brown/Flaming electrode puller. After pulling, the tips of the electrodes were individually broken to obtain an inner tip diameter of 20–40 μm to fit the respective size of the abducens or trochlear nerve, each of which consists of a single branch. The nerves were then sucked into the electrode over a length of about 0.3–0.5 mm. Both extraocular motor nerves contain ~40 axons with a diameter range of ~0.3–3 μm (M. Faust, A. Horn-Bochtler, and Hans Straka, Ludwig-Maximilians-University, Munich, Germany, unpublished results) and allowed recordings of single axons (occasionally), two to three axons, or multiple axons. The spikes of up to three simultaneously recorded axons were distinguishable based on spike shape and amplitude (Dietrich and Straka, 2016). Motion stimuli for natural activation of the horizontal semicircular canals (HCs) consisted of sinusoidal rotations of the turntable around the vertical axis at frequencies of 0.1–1 Hz and peak velocity amplitudes of ±6–60°/s for modulating the spike activity of motoneuronal axons in the abducens nerve. This dynamic range of motion stimuli is well within the physiological range for tadpoles at the developmental stages used for the current experiments (Lambert et al., 2008) and is within the range of motion

kinematics during undulatory swimming (Hänzi and Straka, 2017). Control recordings of the trochlear nerve were performed during horizontal-axis roll motion stimulation at a horizontal position of 45° (for details, see Branoner and Straka, 2015; Dietrich and Straka, 2016). Even though recordings from an individual preparation are possible for up to 3 d (Straka and Simmers, 2012), nerve recordings in the current study were restricted to the same day after preparation to minimize potential variations of experimental conditions.

The contribution of different excitatory and inhibitory neurotransmitter systems and receptor subtypes to the transmission of bilateral vestibular inputs onto abducens motoneurons was studied using focal injections of specific antagonists directly into the abducens nucleus through beveled (30°) glass microelectrodes. The abducens nucleus in rhombomere 5 (r5) was localized using external landmarks such as the lateral entrance/exit of the VIIIth and IXth cranial nerves in r4 and r6, respectively, into the hindbrain and the plainly visible midline along the IVth ventricle. Using a micromanipulator, injection electrodes were inserted vertically into the hindbrain through the ventricular surface, ~150 μm lateral to the visible midline in r5, corresponding to the center of the abducens nucleus. Transmitter receptor antagonists were applied by pressure pulse injection (0.5 bar; 50 ms) of a volume of 20–50 nl, corresponding to a spherical bolus with a diameter of ~300–450 μm. The rather superficial location of the abducens nucleus ~50 μm below the ventricular surface and the likely leakage through the electrode track into the bath solution (Pfanzelt et al., 2008) reduced the amount of injected blockers. The volume nonetheless covered the entire abducens nucleus, which spans across ~200 μm (Fig. 1*A*). To exclude indirect effects of the injected blockers due to potential spread to the neighboring ipsilateral vestibular nuclei at a distance of 500–600 μm from the abducens nucleus and interference with vestibular signal processing, control recordings of the ipsilateral trochlear nerve (distance between abducens and trochlear nucleus: ~1 mm) were made in parallel to those of the abducens nerve. No change in vestibular-evoked trochlear motor activity was encountered after a focal pressure injection of antagonists into the abducens nucleus, indicating that the applied drugs remained confined to the abducens nucleus.

Vestibular-evoked glutamatergic excitation of abducens motoneurons was blocked by focal bolus injections of the AMPA receptor antagonist NBQX (10 μM; Tocris Bioscience) and by the NMDA receptor antagonist D-AP5 (500 μM; Tocris Bioscience) into the abducens nucleus. Focal abducens injections of the glycine receptor antagonist strychnine (10 μM; Tocris Bioscience) and of the $GABA_A$ receptor blocker gabazine (10 μM; Tocris Bioscience) were made to test potential contributions of these inhibitory transmitters to the vestibular-induced modulation of abducens motoneuronal activity. All antagonists were dissolved in frog Ringer's solution.

Data analysis. Peristimulus time histograms (PSTHs) illustrating the average motoneuronal firing patterns over a single cycle of sinusoidal head rotation were obtained from raw data using Spike2 scripts that allowed analyzing the recorded multi-unit or single-unit spike discharge (Dietrich and Straka, 2016). For all stimulus parameters (frequencies, amplitudes), average responses were calculated from at least 10 single cycles. The PSTHs were further processed and analyzed statistically using Microcal Origin 6.0G and MathWorks MATLAB software. PSTHs were normalized and averaged (± SEM) for comparison within and between

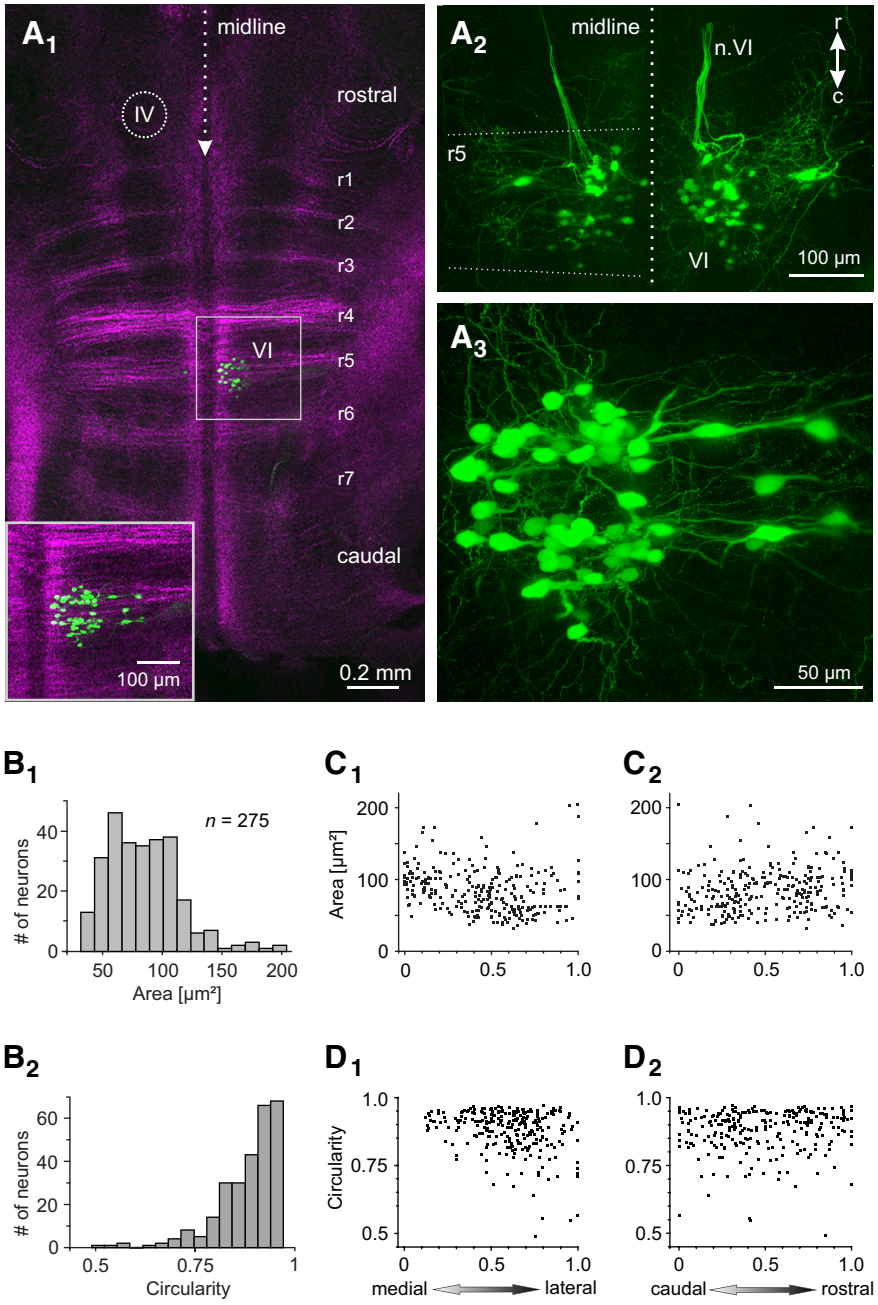

Figure 1. Anatomical organization of the abducens nucleus in larval *X. laevis*. ***A***, Horizontal confocal reconstruction of a hindbrain whole-mount preparation of a stage 54 tadpole depicting retrogradely labeled abducens motoneurons in r5 after unilateral (***A1***, ***A3***) or bilateral (***A2***) application of Alexa Fluor 488 dextran to the VIth motor nerve(s) at the level of the LR muscle; brainstem-crossing fibers, visualized by 633 nm illumination (magenta-colored crossing fibers in ***A1***), indicate the center of r1–7, respectively; inset in ***A1*** is a higher magnification of the outlined area (VI). The location of the trochlear nucleus (IV) is indicated in ***A1***. Note that the two green fiber bundles in *A2* represent the bilateral VIth motor nerves (n.VI) traversing rostrally beneath the ventral surface of the hindbrain. r, rostral; c, caudal. ***B***, Somal size (cross-sectional area, ***B1***) and circularity (***B2***) distributions of retrogradely labeled abducens motoneurons ($n = 275$); circularity of 1 indicates a round cell body. ***C***, ***D***, Dependency of somal size (***C***) and circularity (***D***) on the mediolateral (***C1***, ***D1***) and rostrocaudal (***C2***, ***D2***) motoneuronal position within the abducens nucleus; positions were normalized to the most medial/rostral (0) and most lateral/caudal (1) part of the nucleus, respectively.

different experiments. The dynamics of stimulus-evoked motoneuronal activity was characterized by analyzing the timing of the modulated peak discharge relative to the sinusoidal stimulus; accordingly, phase lead/lag indicated that the peak discharge occurred before/after peak stimulus velocity. The discharge regularity of individual units that were active at rest was quantified using the coefficient of variation 2 (CV2) as described previously (Holt et al., 1996). Spike sorting according to shape and amplitude was performed using principal component analysis included in the Spike2 software.

Anatomy. The location of the principal abducens (VI) nucleus was determined by retrograde labeling of the motoneurons from the LR target muscle in the periphery. The abducens nerve was dissected as for the electrophysiological experiments (above), placed on a thin piece of Parafilm, and covered with a small amount of biocytin crystals (Sigma-Aldrich). After ~10 min, the preparation was rinsed excessively and kept in freshly oxygenated frog Ringer's solution overnight at 12°C as described previously (Straka et al., 2001). Subsequently, the brain was dissected free and fixed in 4% paraformaldehyde in 0.1 M phosphate buffer, pH 7.4, for 4 h at 4°C. To visualize the motoneurons, a standard protocol for processing whole-mount preparations with streptavidin–Alexa Fluor 488 was applied before mounting the preparation in Vectashield mounting medium. The hindbrain region containing retrogradely labeled abducens motoneurons was reconstructed from stacks of ~100–150 consecutive horizontal optical sections after scanning on a Leica SP5–2 confocal microscope at 0.5–1 μm *z*-axis intervals. *z*-axis projections and image processing, as well as quantification of neuronal numbers and measurement of somal cross-sectional areas, were performed using the Fiji software package (Schindelin et al., 2012; http://fiji.sc/wiki/index.php/Fiji). To map the position of retrogradely labeled motoneurons onto the rhombomeric scaffold, all preparations were scanned with an illumination wavelength of 633 nm, visualizing the segmental arrangement of midline-crossing axonal pathways (Chagnaud et al., 2015; Hänzi et al., 2015), thereby outlining the rostrocaudal arrangement of the hindbrain segments.

Eye movement recordings. Eye movements during sinusoidal head rotations were recorded noninvasively from above with a video camera (Grasshopper color; Point Gray Research) and a zoom objective (Optem Zoom 70XL; Qioptiq Photonics) with an adequate lens (M25 × 0.75 + 0.25). Eye motion was captured at a frame rate of 50 Hz with the respective software (FlyCap2) and analyzed offline using a custom video-processing algorithm written in MATLAB to compute eye position over time (for details, see Ramlochansingh et al., 2014). From the raw eye position data, slow drift was removed by high-pass filtering (Gaussian filter, 0.01 Hz). Outliers caused, for example, by resetting fast phases were discarded. The resulting eye position trace was then averaged over all stimulus cycles. The averaged eye position traces over a single cycle were fitted with a sine wave of the same frequency as the stimulus to determine gain and phase of the eye movement. The extracted averaged eye position traces were then used for the computational model.

Computational model. The purpose of constructing a model was to evaluate the respective contributions of dynamically different types of abducens motoneurons to tadpole eye movements. The model uses the measured spike trains from single unit recordings of abducens motoneurons and transforms them into an eye movement by assuming a linear summation of the contributions from single motoneurons. To match approximately the number of spikes for a comparison between silent and spontaneously active neurons, the number of spikes taken into account for the latter neurons was reduced by using only the first quarter of the recorded spikes (or one period, whichever had a longer duration). After this data reduction, the number of spikes between the two groups was not statistically different (repeated-measures ANOVA $p = 0.38$). The response r_a due to a single abducens motoneuron with spike train δ_i (with each spike being represented as a Dirac pulse at time t_i) is constructed as follows:

$$r_a(t) = f\left(\sum \delta_i\right) = \sum f(\delta_i)$$

where $f()$ is the response of a third-order differential equation representing the eye plant combined of muscle activation and eyeball dynamics. The Laplace form of the differential equation is given as follows:

$$F(s) = \frac{1}{1 + \tau_1 s} \cdot \frac{1}{1 + \tau_2 s} \cdot \frac{1}{1 + \tau_{eye} s}$$

where $\tau_1 = 20$ ms, $\tau_2 = 40$ ms, and $\tau_{eye} = 330$ ms. The first two time constants correspond to the muscle activity, which was then processed with a simplified model of the oculomotor plant with time constant τ_{eye}. Because a single abducens motoneuron causes contraction of the LR eye muscle only, we modeled the corresponding motoneuron in the oculomotor nucleus contracting the antagonistic medial rectus eye muscle as having the same spike train but phase shifted relative to the stimulus, resulting in a response r_o. Accordingly, abducens and oculomotor motoneurons act in a push-pull fashion with oppositely oriented directional tuning.

The complete eye movement m was modeled as a weighted sum of single neuron responses as follows:

$$m(t) = \sum w_j \cdot (r_a(t) - r_o(t))$$

where w_j is the weight of one pair of motoneurons. The weights were fitted to the measured eye movements $e(t)$ by a constrained least-squares minimization (MATLAB function "lsqnonneg") minimizing the least-squares error between $m(t)$ and $e(t)$. Note that, for the fit, both $m(t)$ and $e(t)$ traces were resampled to contain 1000 values for one stimulus cycle before fitting to yield equally long durations. Data for four eye movement frequencies (0.1, 0.2, 0.5, and 1 Hz) of each animal were fitted simultaneously to determine the weights of the best-fitting set of neurons for that particular animal. To compare between motoneuronal subtypes, the explained variance was calculated for fits of individual subgroups.

Results

Anatomical organization of abducens motoneurons

Application of biocytin to the LR branch of the abducens nerve in stage 53–54 *X. laevis* tadpoles retrogradely labeled on average ~40 motoneurons (41.2 ± 6.6, $n = 7$) within a single hindbrain nucleus (Fig. 1*A1–A3*). The location of the cell bodies close to the midline in r5 (Fig. 1*A1* and inset) complies with the known monosegmental origin of principal abducens motoneurons in other anuran species (Straka et al., 1998, 2006). Axons of all LR innervating abducens motoneurons joined into a ventrally projecting fiber tract (not seen in the horizontal confocal projection in Fig. 1*A2*), exited the brainstem at the ventral surface of r5 close to the midline as the VIth cranial nerve, coursed rostrally along the pial surface of the brainstem as indicated in Figure 1*A2* by the bilateral axonal fiber bundles (n.VI) and left the cranium laterally along with the Vth and VIIth cranial nerves. Somata of these principal abducens motoneurons (Fig. 1*A3*) were generally round or oval shaped with maximal diameters of 8–30 μm, corresponding to cross-sectional areas that varied considerably over a range of 32–204 μm^2 ($n = 275$) at the plane of their largest perimeter (Fig. 1*B1*,*B2*). The cell size distribution of motoneurons appeared to form a continuum; however, the majority of somata had cross-sectional areas in the range of 50–100 μm^2 even though few very large neurons were encountered regularly (Fig. 1*B1*). Plotting soma size against the mediolateral or rostrocaudal positions of abducens motoneurons revealed that cells of different sizes are more or less equally distributed within the nucleus (Fig. 1*C1*,*C2*). To potentially distinguish distinct motoneuronal subtypes with respect to cell shape, the circularity of the somata (4π * area/perimeter^2) was determined (Fig. 1*B2*). Based on this calculation, most principal abducens motoneurons had round cell bodies (circularity close to 1), with a continuous transition toward few motoneurons with oval-shaped somata

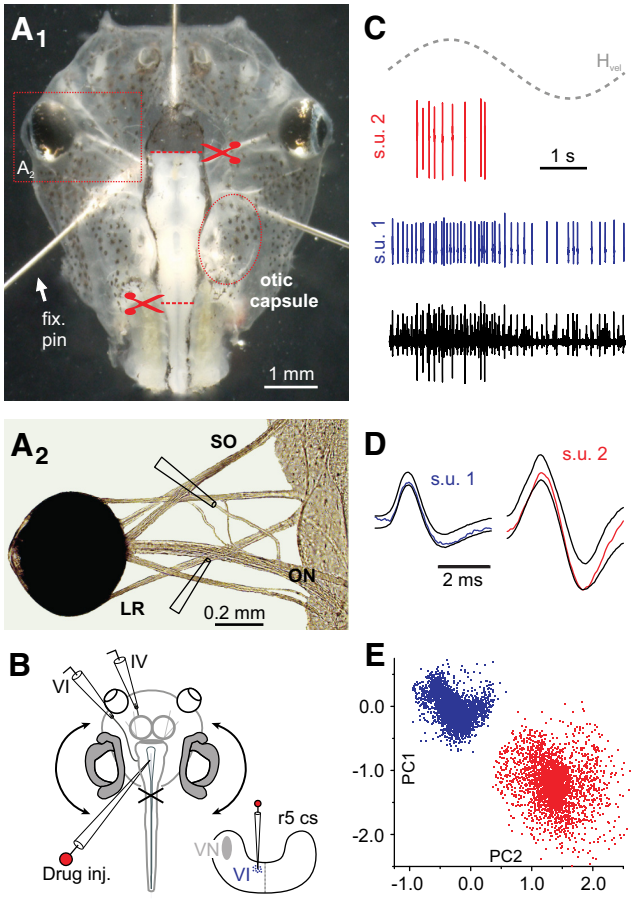

Figure 2. Semi-intact *X. laevis* preparations for electrophysiological recordings and pharmacological perturbations of extraocular motor nerve activity. ***A***, Photomicrographs, depicting in ***A1*** an isolated head of a stage 54 tadpole secured to the Sylgard floor of the recording chamber with three pins (fix. pin), with intact inner ears, CNS, and eyes and, in ***A2***, the extraocular motor innervation of eye muscles. ***B***, Schematics of the semi-intact preparation, indicating LR (VI) and SO (IV) nerve recording electrodes and the pipette for pressure injection of drugs into the abducens nucleus and of a hindbrain cross-section (cs) at r5, depicting the injection electrode path (bottom right); curved double arrows indicate horizontal turntable rotation. ***C***, Representative multiunit abducens nerve discharge (black trace) and the activity of extracted single units (red and blue traces) based on spike shape analysis. ***D***, ***E***, Spike templates (s.u. 1 and s.u. 2 in ***D***) of the two single units isolated in ***C*** and graphical illustration of the principal component analysis (PC1, PC2) used for the spike sorting with respect to spike shape and amplitude (***E***). ON, Optic nerve. Dashed gray sine wave in ***C*** indicates head motion stimulus velocity (H_{vel}). Photograph in ***A2*** was modified from Lambert et al., 2008.

(Fig. 1*B2*). Although motoneurons with round somata predominated at midline positions, motoneurons at increasingly more lateral positions within the nucleus tended to be more oval shaped (Fig. 1*D1*). In contrast, no difference in cell shape with respect to the rostrocaudal position was observed (Fig. 1*D2*).

Spontaneous and motion-evoked discharge profiles of abducens motoneurons

The discharge patterns of abducens motoneurons at rest and during imposed head motion in semi-intact preparations of *X. laevis* tadpoles were studied by recording the axonal spike activity of the abducens nerve after disconnection from its LR target muscle (Fig. 2*A1*,*A2*,*B*). In many recordings, the multiunit discharge of the LR nerve (black trace in Fig. 2*C*) could be dissociated into the spike activity of individual, single units by spike shape discrimination (red and blue traces in Fig. 2*C*) using principal component analysis (Fig. 2 *D*, *E*; see also Dietrich and Straka, 2016). The functionally preserved inner ear end organs in these preparations allowed characterizing discharge dynamics of individual abducens motoneurons at rest and during imposed head rotation (Fig. 3*A1*,*A2*). All isolated motor units ($n = 57$ units from $n = 40$ nerves) had a resting activity below ~10 spikes/s (Fig. 3*B*), including a group of cells ($n = 13$) with spikes of particularly large amplitude in multiunit recordings (cf. blue and red arrowheads in Fig. 3*A2*) that were silent at rest (dark green bar in inset of Fig. 3*B*) but became discernible during motion stimulation. The absent resting activity in the latter neurons impaired immediate detection during recordings and most likely caused an underestimation of their number, which might range well >30%. If these neurons mediate slow phase extraocular motor commands or burst-like signals for fast resetting phases during optokinetic responses and/or spinal efference copy-driven eye movements during swimming in *X. laevis* larvae remains to be determined. At variance with this latter group, spontaneously firing units ($n = 41$) usually had spikes of smaller amplitude with a highly variable resting firing rate that extended over two decades within this group (~0.1–10 spikes/s; Fig. 3*B*), compatible with previous findings in adult ranid frogs (Dieringer and Precht, 1986). The discharge regularity of these neurons covered a correspondingly large range as indicated by the CV2 (Fig. 3*C1*,*C2*). For motor units with resting rates between 1 and 10 spikes/s, the average interspike interval was linearly correlated with the CV2 ($r^2 = 0.113$; Fig. 3*C2*).

During horizontal sinusoidal rotation, the vast majority of abducens motoneurons became cyclically active, in phase with the velocity of contraversive head movements (right traces in Fig. 3*A1*,*A2*). To facilitate a classification of responses, the discharge rates of different units were normalized before population averages were calculated. Athough the firing rate modulation during sinusoidal motion generally increased in depth with stimulus velocity, the threshold for this modulation varied considerably between different motoneurons (Fig. 3*D1*,*D2*). In fact, motor units that were silent ("s") at rest had relatively high stimulus velocity thresholds (28.8 ± 3.5°/s; $n = 16$; inset in Fig. 3*D2*,*E*), whereas spontaneously active motor units ("sa") exhibited a cyclic discharge modulation (Fig. 3*D1*) above a significantly ($p < 0.001$; Mann–Whitney *U* test) lower stimulus peak velocity of the sinusoidal motion (1.9 ± 0.8°/s; $n = 41$; inset in Fig. 3*E*). This difference was not surprising because abducens motoneurons in monkeys also display a similar correlation between resting rate and response threshold (Broussard et al., 1995). Importantly however, the detailed analysis of *X. laevis* abducens motoneuronal responses patterns revealed a more or less continuous range of discharge modulation depths at ±30°/s stimulus peak velocity. In fact, this parameter correlated linearly with the rate of the resting discharge of the respective motoneurons (Fig. 3*E*, $r^2 = 0.154$), suggesting a continuum of motoneurons with respect to resting rate, discharge regularity, and sensitivity to motion stimuli.

Apart from the generally similar VOR response pattern shared by the majority of motor units, amplitude and phase analyses of sufficiently long periods of recordings during horizontal sinusoidal head motion ($n = 35$) allowed a more detailed characterization and classification of abducens motoneuronal response properties. Independent of the distinguishing traits (below), all tested motoneurons with a spontaneous resting rate ($n = 22$) exhibited peak firing rates that increased steadily with increasing stimulus magnitude up to ~25 spikes/s and saturated above a peak velocity of ±60°/s at 0.5 Hz (Figs. 3*D1*, 4*A1*,*A2*, and black and red lines in Fig. 4*C1*). The peak response within a given

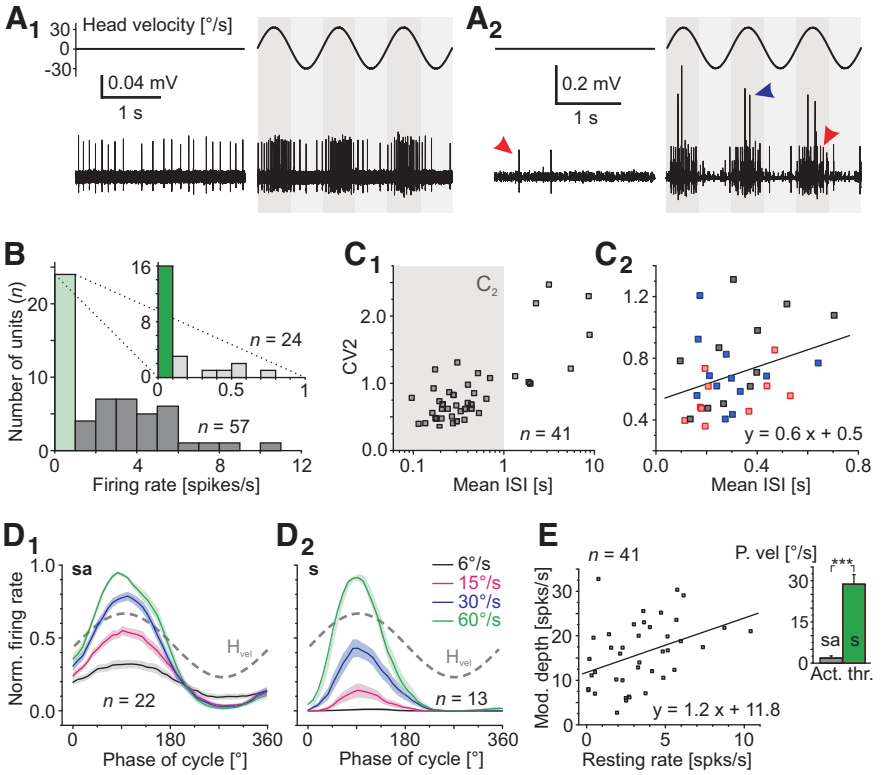

Figure 3. Discharge properties of silent and spontaneously active abducens motor units. ***A***, Representative examples of units with moderate (***A1***) and low (red arrowheads in ***A2***) spontaneous activity and a typical silent unit (blue arrowhead in ***A2***) at rest (left traces in ***A1***, ***A2***) and during multiple cycles of horizontal sinusoidal head rotation (right traces in ***A1***, ***A2***). ***B***, Histogram depicting the distribution of neuronal firing rates at rest; the distribution between 0 and 1 spikes/s (light green bar) is plotted at an extended scale in the inset; the dark green bar indicates units that were silent at rest. ***C***, Correlation between the mean interspike interval (ISI) and CV2 in ***C1*** for all spontaneously active units and in ***C2*** for units with a resting discharge between 1 and 10 Hz (gray area in ***C1***; $n = 33$). Color code in ***C2***: Red, Group I units, blue: Group II units, black: unspecified units recorded only at a single motion stimulus frequency (0.5 Hz). ***D***, Average firing rate modulation (±SEM, shaded areas) of a population of spontaneously active (sa; ***D1***) and silent (s; ***D2***) motor units over a single motion cycle at 0.5 Hz and different stimulus peak velocities. ***E***, Linear correlation between the resting rate and modulation depth of spontaneously active neurons during rotation at 0.5 Hz with a peak velocity of ±30°/s ($n = 41$). Inset depicts differences in activation threshold (Act. thr.) between silent (s) and spontaneously active (sa) units. Dashed gray sine waves in ***D*** indicate head motion stimulus velocity (H_{vel}).

motion cycle was approximately in phase with stimulus velocity, independent of its magnitude (black and red lines in Fig. 4*C3*).

Although the response profile during increasing peak velocities was essentially indistinguishable among spontaneously active motoneurons, a categorization into two subgroups with respect to the timing of the peak response became obvious when the stimulus frequency was systematically altered while the peak velocity was kept constant at ±30°/s (Fig. 4*A*,*B*). Motor units of the first subgroup (Group I; $n = 12$; Fig. 4*A1*) exhibited modulated responses during sinusoidal rotation with a peak firing rate that was maximal at a rotational frequency of 0.2 Hz and decreased with increasing stimulus frequency (black line in Fig. 4*C2*). Importantly, the decrease of the peak response rate in these motor units was accompanied by a large concurrent shift of the timing of the response peak from a phase lead of ~40° at 0.1 Hz (i.e., maximal discharge is reached before the stimulus peak) to a phase lag of ~40° at 1 Hz (i.e., maximal discharge is reached after the stimulus peak) (black line in Fig. 4*C4*). In contrast, motor units of the second subgroup (Group II; $n = 10$; Fig. 4*A2*) exhibited responses that decreased only slightly with increasing stimulus frequency, whereas the phase relation between response and stimulus remained constant (red lines in Fig. 4*C2*,*C4*). In summary, the two abducens motoneuronal subgroups appear to be similarly motion sensitive with respect to head velocity but differ considerably in the amplitude and temporal signature of the responses when stimulus frequencies are altered.

To test whether the frequency-sensitivity of Group I abducens motoneurons reflects a response sensitivity to the different motion amplitudes (position sensitivity), an additional set of stimuli was applied that provoked eye movements to the same eccentric position but with different frequencies. The respective stimulus parameters were determined before the abducens nerve recordings using eye motion video recordings in semi-intact preparations with both eyes intact but in the absence of visual input. Sinusoidal stimuli with 0.1 Hz and a maximal displacement of ±16.6° (corresponding to ~±10°/s peak velocity) drove the eye to the same eccentric position as 0.2 Hz and ±11° displacement, 0.5 Hz and ±10° displacement and 1 Hz and ±10° displacement ($n = 6$). This set of "constant amplitude" rotational stimuli was subsequently used to test responses of identified Group I abducens motor units that, in case of a potential position rather than frequency sensitivity, would display similar peak firing rates during each of these stimulus parameters. However, instead, all recorded Group I motoneurons responded differentially to the four stimulus conditions with respect to both the amplitude and timing of the peak discharge (note the change in response in Fig. 4*A1*, right, $n = 8$). This suggests that Group I motoneurons indeed encode the frequency but not the amplitude of eye movements. As a control, the "constant amplitude" stimulation was also applied to some Group II motoneurons (Fig. 4*A2*, right, $n = 4$) that were also insensitive to the eye motion amplitude.

The differentiation into two categories was not limited to spontaneously active units with low stimulus thresholds but was also encountered in a comparable manner for those neurons that were silent in the absence of motion stimuli ($n = 13$; Figs. 3*A2*,*D2*, 4*B1*,*B2*). Common to all of these latter units was the presence of a sharp response peak during contraversive head motion (Fig. 3*D2*). Even though the discharge modulation at ±30°/s peak velocity was relatively weak (12.6 ± 1.3 spikes/s), changes in stimulus velocity were precisely encoded once the activation threshold was reached (Fig. 3*D2*). However, given the absence of a spontaneous resting rate, these neurons only encoded the excitatory but not the inhibitory component of the VOR. Similar to the situation in spontaneously active motor units, differences in discharge profiles were mainly observed upon changes in stimulus frequency (Fig. 4*B1*,*B2*,*D2*,*D4*). Here again, the response modulation during sinusoidal head rotation in Group I motoneurons ($n = 7$) changed in amplitude with increasing motion frequency, accompanied by a concurrent shift of the response peak from a phase lead of ~40° at 0.1 Hz to a phase lag of ~35°/s at 1 Hz (Fig. 4*B1*, black line in Fig. 4*D4*). Silent Group II mo-

toneurons ($n = 6$) exhibited peak responses of similar magnitude and timing independent of stimulus frequency (black and red lines in Fig. 4*B2*), as observed for the corresponding class of spontaneously active motoneurons. However, a modulated spike discharge in the silent neurons could not be triggered with motion stimuli that had peak velocities $\leq \pm 30$°/s (Fig. 4*D1*) or frequencies >0.2 Hz at ± 30°/s (Fig. 4*D2*). Therefore, independent of the presence or extent of spontaneous activity, abducens motoneurons separate into two groups that generate motor commands that are either in phase with the velocity of the sinusoidal head motion stimulus or are dependent in their response amplitude and timing on the stimulus frequency.

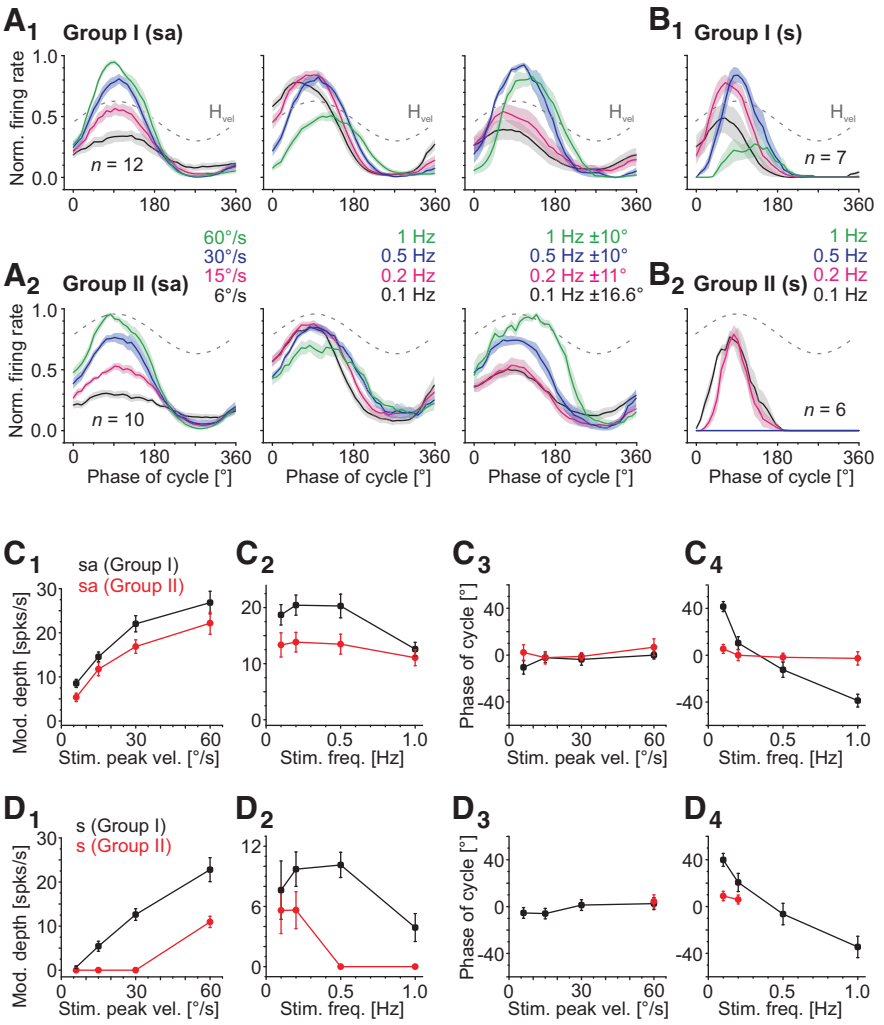

Figure 4. Discharge properties of Group I and Group II abducens motor units. ***A***, ***B***, Average rotation-evoked firing rate modulation (±SEM, shaded areas) of spontaneously active (sa) Group I (***A1***, $n = 12$) and Group II (***A2***, $n = 10$) and silent (s) Group I (***B1***, $n = 7$) and Group II (***B2***, $n = 6$) motor units over a single rotation cycle at a stimulus frequency of 0.5 Hz and varying peak velocities (left in ***A1***, ***A2***), at a stimulus peak velocity of ±30°/s and varying frequencies (middle in ***A1***, ***A2***; ***B1***, ***B2***) and at different peak amplitude/frequency combinations that always drive the eye to the same eccentric position (right in ***A1***, ***A2***); dashed gray sine waves indicate head motion stimulus velocity (H_{vel}). ***C***, ***D***, Dependency of the maximal discharge modulation depth (***C1***, ***C2***, ***D1***, ***D2***) and phase *re* stimulus velocity (***C3***, ***C4***, ***D3***, ***D4***) of rotation-evoked responses (±SEM) on stimulus peak velocity (***C1***, ***C3***, ***D1***, ***D3***) and frequency (***C2***, ***C4***, ***D2***, ***D4***) in spontaneously active (***C***) and silent (***D***) Group I (black) and Group II (red) motor units.

Motion-insensitive abducens motoneurons

In addition to the majority of motion-sensitive abducens motor units, a small population of neurons ($n = 6$) was encountered in different preparations that had no spontaneous spike activity, displayed an occasional burst-like discharge (Fig. 5*A1*,*A2*), and in multiunit recordings exhibited the largest spikes (asterisks in Fig. 5*B*). In contrast to the head motion-sensitive abducens motoneurons described above, these neurons were unresponsive to imposed horizontal rotations but instead often bursted randomly during table motion (Fig. 5*A2*, asterisks in Fig. 5*B*). The absence of any correlation between bursting and rotational stimuli was confirmed by the average activity over a single motion cycle (Fig. 5*A3*). Compatible with the obvious absence of vestibular influence, these motor units continued to fire occasional bursts of spikes (bottom trace in Fig. 5*C*) after transection of the contralateral VIIIth nerve, a perturbation that consistently caused complete elimination of the robust cyclic activity of motion-sensitive abducens motor units (cf. top and bottom traces in Fig. 5*C*). Even though the activity of these motion-insensitive units is reminiscent of that of accessory abducens motoneurons (Dieringer and Precht, 1986), the distinct isolation of the identified LR nerve branch close to the target muscle in our experiments makes a recording of such motoneurons unlikely. More likely, motion-insensitive units form a particular class of principal abducens motoneurons that are only activated during optokinetically driven fast resetting eye movements (Schuller et al., 2014) or by locomotor efference copies, known to recruit extraocular motoneurons directly during undulatory swimming in *X. laevis* tadpoles (Lambert et al., 2012).

Vestibular inputs to abducens motoneurons

Bilateral vestibular inputs to vertebrate abducens motoneurons consist of a crossed excitation and an uncrossed inhibition (Precht, 1978). To reveal potential differences in the pharmacological profile of the two different groups of abducens motor units, we tested the specific recruitment of transmitter receptor subtypes during motion-driven extraocular motor activity.

Glutamatergic excitatory inputs

The contribution of AMPA and NMDA receptors to motion-induced discharge modulation of abducens motor units was tested by focal pressure injection of specific transmitter blockers (AMPA receptor blocker: NBQX; NMDA receptor blocker: D-AP5) into the abducens nucleus, respectively (Fig. 2*B*). Independent of the previously established classification of spontaneously active motor units into Group I and II, bolus injections of either D-AP5 (500 μM) or NBQX (10 μM) caused a significant reduction of the spontaneous discharge. The almost instantaneously occurring reduction of the motoneuronal discharge after the injection usually lasted for 10–15 min and was followed by a gradual recovery that reached control values ~45 min after injection of D-AP5, whereas the effect of NBQX was only partially

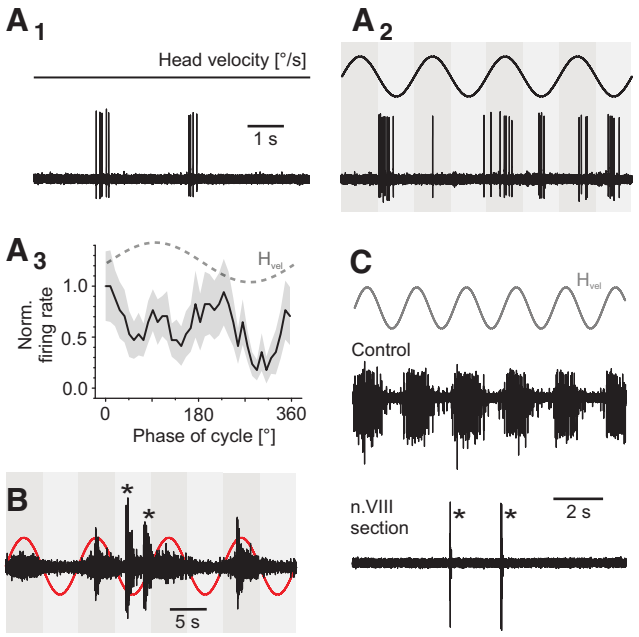

Figure 5. Discharge properties of non-VOR abducens motor units. ***A***, Representative example of a non-VOR unit at rest (***A1***) and during sinusoidal head rotation over multiple rotation cycles at 0.5 Hz and ±60°/s peak velocity (***A2***) with its average response over a single cycle (***A3***). ***B***, Representative example of a multiunit abducens nerve discharge during multiple cycles of head rotation at 0.5 Hz and ±30°/s peak velocity. Note that non-VOR units (*) have the largest spike amplitudes. ***C***, Representative example of a multiunit abducens nerve discharge during multiple rotation cycles before and after contralateral VIII th nerve transection. Note that a single non-VOR unit remains active after the lesion (*). Dashed sine waves in ***A3*** and red and gray sine waves in ***B*** and ***C*** indicate head motion stimulus velocity (H_{vel}). Calibration bar in ***A1*** also applies to ***A2***.

reversible. Both blockers reduced the spontaneous abducens nerve activity ($n = 7$), but D-AP5 was significantly more effective than NBQX. Although the NMDA blocker decreased the spontaneous discharge rate of single abducens motor units to ~40% (37.2 ± 8.5%) of the control value, NBQX had a significantly smaller effect and reduced the resting rate only to ~75% (75.5 ± 5.8%; $p = 0.0156$; Wilcoxon signed-rank test) of the control.

During sinusoidal head rotation, the excitatory response component of all recorded single units in controls (black traces in Fig. 6*A*,*B*), independently of the presence and extent of spontaneous activity, was consistently reduced after injection of either of the two glutamate receptor blockers (red and blue traces in Fig. 6*A*,*B*), whereas control recordings of the trochlear nerve remained unchanged (Fig. 6*G*). Notably, the relative magnitudes of the unmasked AMPA and NMDA receptor-mediated response components differed between Group I and II abducens motoneurons. This differential impact was quantified by comparing the change in the area under the average modulated response curve (integral) over a single cycle before (black traces in Fig. 6*C*,*D*) and after injection of the respective drug (red and blue traces in Fig. 6*C*,*D*). Independent of the presence and/or extent of spontaneous resting activity, D-AP5 reduced the excitatory response component in Group I abducens motor units ($n = 8$) by >80%, whereas the NBQX-provoked decrease amounted to only ~60% of the control response (representative examples are shown in Fig. 6*C1*,*C2*). Accordingly, the residual AMPA response component after D-AP5 injection was significantly smaller (16.4 ± 6.1%; $p = 0.0078$; Wilcoxon signed-rank test) than the NMDA component after NBQX injection (42.4 ± 7.8%; Fig. 6*E1*,*E2*). This suggests that the cyclic discharge modulation of these motoneurons during sinusoidal motion stimulation is predomi-

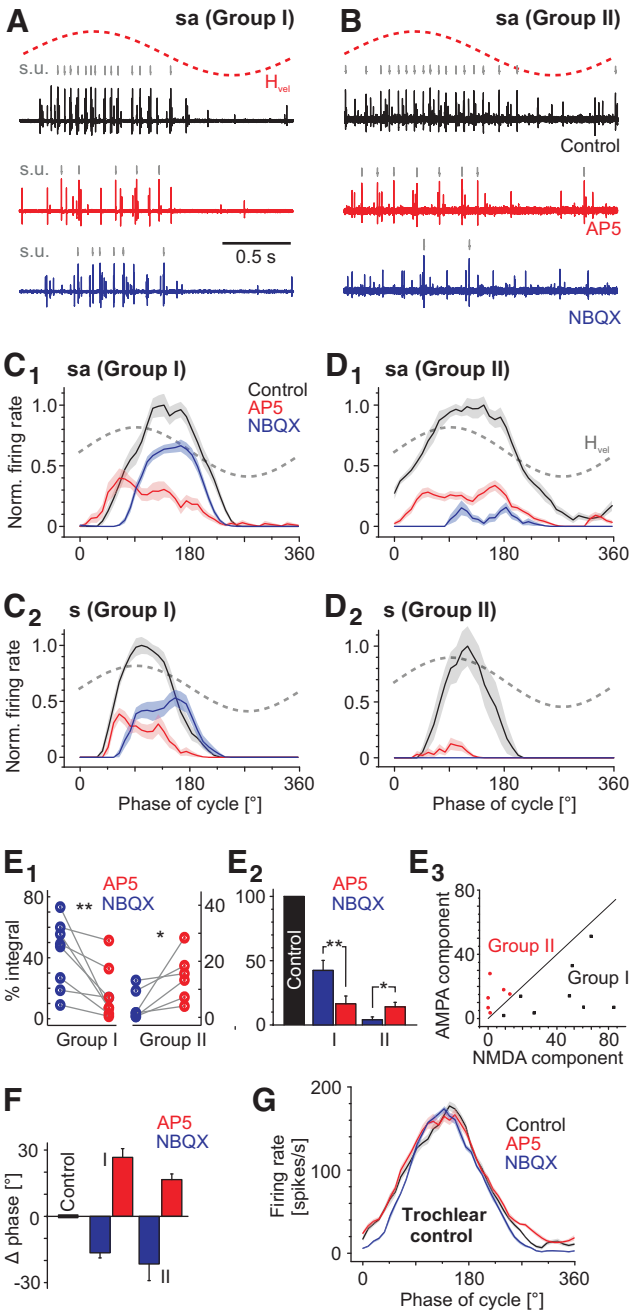

Figure 6. Excitatory neurotransmitter profile of Group I and Group II abducens motor units. ***A***, ***B***, Representative examples of spontaneously active Group I (***A***) and Group II (***B***) units before and after focal injection of D-AP5 (red, 500 μM) and NBQX (blue, 10 μM) into the respective abducens nucleus. Single units (s.u., gray traces) were identified by spike sorting. ***C***, ***D***, Average normalized firing rate modulation over a single rotation cycle (±SEM, shaded areas) of representative spontaneously active (sa; ***C1***, ***D1***) and silent (s; ***C2***, ***D2***) Group I (***C***) and Group II (***D***) abducens motor units at a stimulus frequency of 0.5 Hz and peak velocity of ±30°/s before and after D-AP5 (red) and NBQX (blue) injection into the respective abducens nucleus. ***E***, Dot plot illustrating the relative change in the area under the curve after D-AP5 and NBQX injection for individual Group I and II motoneurons (***E1***); bar charts depicting the average (±SEM) residual components of the respective response integrals (***E2***) and correlation of AMPA and NMDA components in Group I (black) and II (red) motoneurons (***E3***); note that the separation line has a slope of 1. ***F***, Phase shifts of the response peaks after NMDA (D-AP5, red) and AMPA (NBQX, blue) receptor blockade in spontaneously active (sa) and silent (s) Group I and Group II abducens motoneurons. ***G***, Representative example of a trochlear control recording before and after D-AP5 and NBQX injection into the abducens nucleus. Dashed gray sine waves in ***A***–***D*** indicate head motion stimulus velocity (H_{vel}).

nantly driven by NMDA receptor-mediated excitation, with a smaller contribution of AMPA receptors (Fig. 6*E1*,*E2*). In contrast, in Group II motor units ($n = 6$), NBQX had a larger impact on the excitatory response than D-AP5 and reduced the response by ~95%, whereas the NMDA blocker caused a reduction by ~85% (representative examples in Fig. 6*D1*,*D2*). Therefore, despite the considerable efficiency of both blockers, the residual NMDA response component after NBQX injection was significantly smaller (4.0 ± 2.2%; $p = 0.0313$; Wilcoxon signed-rank test) compared with the AMPA component after D-AP5 injection (14.0 ± 3.5%; Fig. 6*E1*,*E2*). In fact, NBQX usually abolished the evoked responses completely in those Group II units that were silent at rest (blue trace in Fig. 6*D2*), whereas a small response component persisted in spontaneously active Group II motor units after injection of the AMPA receptor blocker (blue trace in Fig. 6*D1*).

These results suggest that excitatory responses during motion stimulation in the two groups of abducens motoneurons are differentially organized with respect to glutamate receptor subtypes. Whereas Group II motoneurons are predominantly excited by AMPA receptors, Group I motoneurons are mainly activated by an NMDA receptor-mediated component during motion stimulation. This becomes especially obvious when plotting the residual response magnitude after pharmacological inactivation of either the NMDA or AMPA component independent of a prior classification of neurons into Group I or II (Fig. 6*E3*): the line with a slope of 1 (Fig. 6*E3*) distinctly separates Group I (black dots) from Group II motoneurons (red dots in Fig. 6*E3*), indicating that the proportions of activated AMPA/NMDA components are inversely related in the two groups of abducens motoneurons.

Independent of the relative contributions of AMPA and NMDA receptors to the excitation of Group I and II abducens motoneurons, the pharmacological block of the two components also affected the timing of the response peak differentially (Fig. 6*C1*,*C2*,*D1*,*F*). Compared with controls (black traces in Fig. 6*C*,*D*), application of NBQX caused a delay of the response peak with respect to the sinusoidal stimulus in all tested motor units (blue traces in Fig. 6*C1*,*C2*,*D1*). This resulted in a considerable phase lag of the evoked responses by 15–20° and was particularly pronounced in Group II motoneurons (blue bars in Fig. 6*F*). In contrast, application of D-AP5 provoked an opposite shift of the response peak of similar magnitude (red traces in Fig. 6*C1*,*C2*, *D1*,*D2*), thereby generating a pronounced phase lead of the modulated responses during the block (red bars in Fig. 6*F*). Therefore, the timing of the peak responses was either delayed (after NBQX application) or advanced (after D-AP5 application) compared with controls. These reciprocal shifts of the response timing after separate blockade of the two glutamatergic receptor subtypes were independent of stimulus velocity or frequency and suggest that the phase relation of vestibular-driven responses in abducens motoneurons is controlled differentially by AMPA and NMDA receptors.

GABAergic and glycinergic inhibitory inputs

The contribution of uncrossed inhibitory HC inputs to abducens motoneurons was first evaluated by surgical removal of the ipsilateral HC sensory epithelium. This ablation immediately caused a substantial increase in the abducens nerve resting activity from ~40 to ~55 spikes/s (38.9 ± 5.8 to 56.7 ± 4.4 spikes/s; $n = 3$), compatible with the notion that, when the head is stationary, a tonic inhibitory input from the ipsilateral HC balances the concurrent tonic excitatory drive from the contralateral side. The augmentation in spontaneous firing rate was accompanied by an increased spike activity of the modulated multiunit abducens nerve discharge over the entire head motion cycle (Fig. 7*A*,*B*). The difference to control responses, however, was particularly obvious during rotation toward the ipsilesional side (Fig. 7*B*, asterisk), in agreement with the loss of an uncrossed inhibition in the absence of ipsilateral HC inputs.

In a separate set of experiments, the uncrossed HC-derived inhibition of abducens motoneurons was further characterized by a longitudinal midline section between r1 and r8 (Fig. 7*C*; Lambert et al., 2012) that removed crossed excitatory HC inputs, as well as a potential amplifying effect of vestibular commissural pathways on vestibulo-ocular signal processing (Malinvaud et al., 2010). The spontaneous discharge of the LR nerve ceased immediately after the surgical invention, but regained a small resting spike activity after 15–30 min. The restored spontaneous firing of abducens motoneurons was cyclically attenuated in a stimulus velocity-dependent manner during sinusoidal rotation in the direction of the ipsilateral HC (Fig. 7*D*, $n = 6$), illustrating the functional impact of the isolated uncrossed vestibular inhibition. A putatively differential contribution of glycine and $GABA_A$ receptors to the inhibitory component of motion-induced discharge modulation was further evaluated by focal pressure injections of the respective antagonists strychnine and gabazine into the abducens nucleus.

Focal injections of strychnine (10 μM) into the abducens nucleus generally resulted in a rather inconsistent, temporarily variable, and often fluctuating elevation of the firing rate around which the LR nerve discharge was modulated during sinusoidal rotation. In addition, strychnine often caused extensive and unpredictable bursts and/or repetitive discharge oscillations during head motion, as described previously (Straka and Dieringer, 1993), likely due to an unmasking of excessive excitatory inputs, thus preventing a quantification of the impact of blocked glycinergic transmission. To reduce the overall amount of excitatory drive to abducens motoneurons, in particular from the contralateral vestibular nucleus, and to exclude a potential commissural influence on vestibulo-ocular signal processing, strychnine injections were repeated in preparations with a longitudinal midline transection. As described above, the multiunit abducens nerve firing rate modulation was strongly reduced compared with control values (blue and black traces, respectively, in Fig. 7*E*, inset in Fig. 7*F*), lacking the excitatory component that derives from the contralateral HC. Nonetheless, subsequent focal application of strychnine eliminated the observed residual inhibitory firing rate modulation during the half cycle of ipsiversive rotation (representative example and average PSTH in Fig. 7*E*,*F*, $n = 6$), indicating, in compliance with previous assumptions (Straka and Dieringer, 1993), that glycine mediates the uncrossed inhibitory component of the horizontal angular VOR.

Focal application of the $GABA_A$ receptor blocker gabazine (10 μM) into the abducens nucleus of unimpaired preparations (without longitudinal midline section) increased the spontaneous abducens nerve discharge considerably, but without causing oscillatory bursting as observed after strychnine injections. The single-unit and/or multiunit abducens nerve resting rate increased by ~130% ($p = 0.0313$; Wilcoxon signed-rank test) from 10.6 ± 2.9 spikes/s in controls to 24.6 ± 7.8 spikes/s after gabazine application ($n = 6$). In addition, the peak firing rate of individual units during sinusoidal motion stimulation at a peak velocity of ±30°/s increased by ~50% (Fig. 7*G*,*H*). Notably, the absolute gabazine-evoked increases in single-unit peak firing rates were essentially independent of the stimulus peak velocity up to ±30°/s (inset in Fig. 7*H*, $n = 7$). The relatively smaller increase observed for responses elicited by higher stimulus

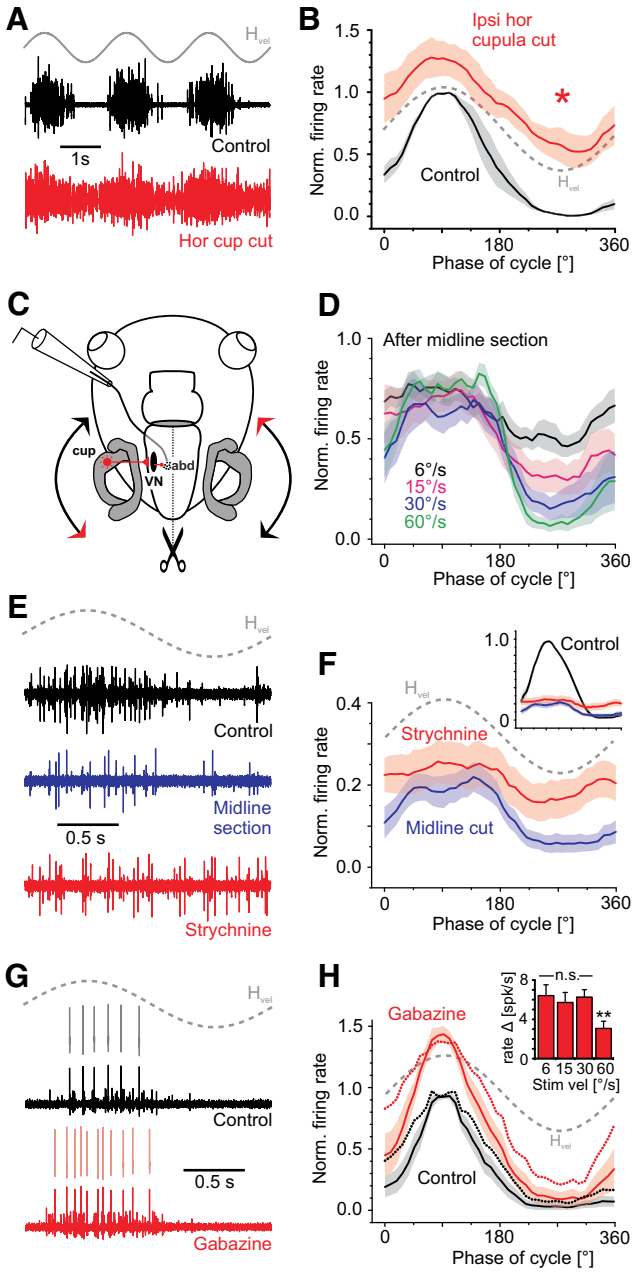

Figure 7. Inhibitory neurotransmitter profile of abducens motor units. ***A***, ***B***, Representative example of a multiunit abducens nerve discharge over multiple rotation cycles (***A***) and average responses (***B***) over a single cycle ($n = 3$, ±SEM, shaded areas) before (black) and after surgical removal of the ipsilateral horizontal (hor) canal cupula (red). ***C***, Schematic of a semi-intact preparation depicting the recording and stimulation paradigm, ipsilateral neuronal VOR connections and the removal of crossed excitatory vestibular inputs to abducens motoneurons by midline section (dotted line). ***D***, Inhibitory modulation of average multiunit abducens nerve responses over a single motion cycle ($n = 6$, ±SEM, shaded areas) at 0.5 Hz and different stimulus velocities of head rotation after midline section. ***E***, ***F***, Representative example (***E***) and average responses (***F***) over a single motion cycle ($n = 6$, ±SEM, shaded areas) of the multiunit abducens nerve discharge before (control, black) after midline section (blue) and subsequent focal strychnine (10 μM) injection into the respective abducens nucleus (red). For comparison, average control responses over a single rotation cycle in the intact preparation are indicated in the inset in ***F***. ***G***, ***H***, Representative example (***G***) and average responses (***H***) over a single motion cycle ($n = 7$ single units, ±SEM, shaded areas) of isolated single units before (black) and after focal injection of gabazine (10 μM) into the respective abducens nucleus. Dotted lines in ***H*** represent average responses of spontaneously active units (three of seven). The bar chart in the inset in ***H*** shows the average increase in firing rate of all single units ($n = 7$, ±SEM) at different peak stimulus velocities (at 0.5 Hz). abd, Abducens; cup, cupula; VN, vestibular nucleus. Gray (dashed) sine waves in ***A***, ***B***, and ***E***–***H*** indicate head motion stimulus velocity (H_{vel}).

intensities suggests that peak firing rates reached a maximum, compatible with the assumption that saturation of single-unit response amplitudes occurs at peak velocities of ~±60°/s (Fig. 4*C1*). Moreover, blocking $GABA_A$ receptors elevated the level around which the discharge was modulated during head rotation and thus caused an augmentation of both the excitatory and inhibitory response components. In these experiments, relatively more single units with no or very low resting rates were recorded (four of seven) that only fired spikes during head rotation in the on-direction (Fig. 7*G*). Therefore, on average, an increase in firing rate was mainly observed for the excitatory half-cycle; that is, during contraversive rotation (solid lines in Fig. 7*H*). However, motor units with a spontaneous resting activity (three of seven; dotted lines in Fig. 7*H*) displayed a considerable increase in activity over the entire motion cycle, suggesting the presence of a tonic $GABA_A$ receptor-mediated inhibition that, in contrast to the glycinergic inputs described above, is independent of modulated ipsilateral vestibular inputs.

In summary, this corroborates previous findings (Spencer et al., 1989; Straka and Dieringer, 1993) showing that glycine and not GABA mediates the transmission of inhibitory vestibular inputs onto abducens motoneurons. In addition, a tonic GABAergic input significantly attenuates abducens motoneuronal firing both at rest and during motion-related vestibular activation.

Computational modeling

To evaluate the relative contributions of the different subgroups of abducens motoneurons to eye movements, a computational model was constructed and used to simulate eye movements with weighted sums of individual muscle contractions caused by single motor unit activity. As a first step, eye motion during horizontal head rotation (±30°/s peak velocity) was video recorded ($n = 7$; Fig. 8*A*) and averaged over a single motion cycle for different frequencies (representative examples in Fig. 8*B*). Evoked eye movements were fitted with a sine wave (blue lines in Fig. 8*B*) that allowed calculating the phase relation of the responses with respect to the stimulus. This analysis revealed that the phase of sinusoidal motion-driven eye movements leads turntable position during low-frequency head rotation (0.1 Hz) and gradually becomes more aligned with the stimulus at higher frequencies (0.5 and 1 Hz; Fig. 8*B*). Therefore, eye movements (green lines in Fig. 8*B*) counteracted table motion (gray lines in Fig. 8*B*) in a stimulus frequency-dependent manner, with concurrently decreasing motion amplitudes (cf. 0.5 and 1 Hz in Fig. 8*B*).

The recorded eye motion was simulated using modulated firing patterns of individual abducens motor units during horizontal head rotation. Spike times were extracted from single-unit recordings (left plot in Fig. 8*C*) and fed into a simplified model of the oculomotor plant (Materials and Methods) to generate contraction patterns of individual muscle fibers (middle plot in Fig. 8*C*) and to compute the weighted sum of the latter to optimally simulate each of the recorded eye movements ($n = 7$). The relative contributions of Group I and Group II motoneurons to the generation of eye movements were evaluated using simulations of the discharge patterns of different combinations of the two groups (Fig. 8*D*). Across stimulation frequencies, the contribution of Group II motoneurons (magenta lines in Fig. 8*D*) was significantly larger than that of Group I motoneurons (blue lines in Fig. 8*D*), although, at higher frequencies, Group I motoneurons became increasingly more important (e.g., cf. 0.1 and 1 Hz in Fig. 8*D*). To quantify the contributions of different types of motoneurons, average explained variances were calculated either for all units, units of one of the two subgroups, or silent or spon-

taneously active units (Fig. 8*E*). The explained variance was highest using all units for simulation (92.1%). Group II motoneurons contributed more to the average explained variance (77.9%) than Group I motoneurons (37.8%). In addition, comparing silent and spontaneously active units revealed that active units contributed somewhat more than silent units to the overall fit (active 67.8% vs silent 54.5%); however, this difference was not statistically significant ($p = 0.62$). To further quantify the role of different types of motor units to explain the observed eye movements, the above simulations were repeated using each of these types alone. Repeated-measures ANOVA of logarithmic least-squares error values to obtain a normal distribution revealed that, depending on the classification scheme (Group I/Group II, active/silent), each of the different populations are differently suited to fit the observed eye movements ($F_{(4,24)} = 4.14$; $p = 0.011$), with the best result for Group II units followed by spontaneously active units. The outcome of the simulation suggests that all types of abducens motoneurons contribute to the final VOR output and conjointly create the spatiotemporal precision of counteractive eye movements. However, Group II motoneurons appear to play a more dominant role compared with those of the Group I subtype, whereas spontaneously active units contribute to eye motion relatively more than motoneurons that are silent at rest, at least during sinusoidal rotations at frequencies between 0.1 and 1 Hz.

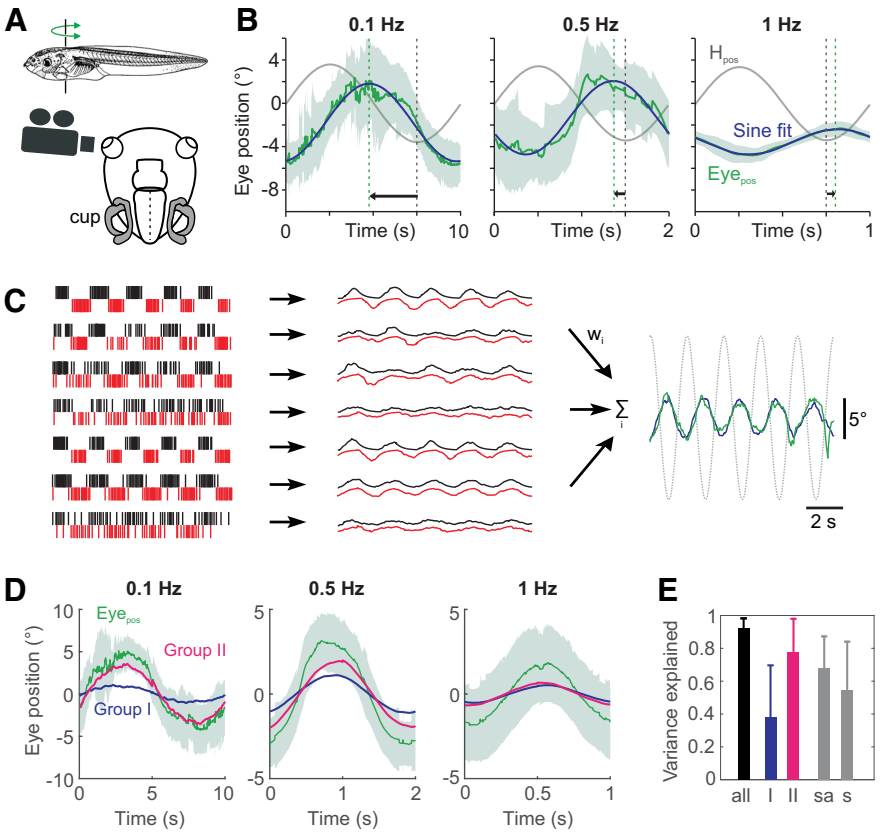

Figure 8. Computational modeling of eye movements. ***A***, Schematic depicting video recordings of eye movements in semi-intact *X. laevis* tadpole preparations during horizontal sinusoidal head rotation. ***B***, Averaged eye positions (green, Eye_{pos}) and corresponding sinusoidal fits (blue, sine fit) over a single cycle of sinusoidal head rotation at three different frequencies (at ±30°/s peak velocity). ***C***, Schematic view of the model used to evaluate whether observed motoneuronal spike patterns sufficiently explain eye movement behavior. Left, Spikes recorded from different motoneurons; black: original recordings; red: 180° shifted version to account for the innervation of the antagonistic muscle. Middle, Time courses of simulated muscle contractions derived from spike trains in the left column. Right, Weighted sum (positive weights, w_i) of muscle contractions fitted to original VOR eye movement recordings (green trace) in response to head rotation (black dashed trace) and resultant simulations of eye movements (blue trace). ***D***, Contributions of Group I (blue) and Group II (magenta) motor units to the simulation of actual eye movements (green, Eye_{pos}) at 0.1, 0.5, and 1 Hz head rotation. ***E***, Explained variances for eye movement simulations from all neurons (black) and contributions of Group I (blue), Group II (magenta), spontaneously active (sa, gray), or silent (s, gray) abducens motor units to overall explained variance. Gray sine waves and dashed black/green vertical lines in ***B*** indicate head motion stimulus position (H_{pos}) and phase relation of the responses, respectively.

Discussion

The principal abducens nucleus in larval *X. laevis* consists of a morphologically heterogeneous population of ~40 motoneurons. Based on differences in discharge profiles during head motion, abducens motoneurons distinguish into two subgroups. Responses of Group I motoneurons have a phase relation and peak firing rate that changes systematically with rotation frequency. In contrast, responses of Group II motoneurons are characterized by high phase precision relative to stimulus velocity that is independent of the frequency. Although AMPA and NMDA receptors contribute differentially to the vestibular-driven excitation of the two neuronal subgroups, a tonic GABAergic and modulated glycinergic vestibular inhibition is present in both populations (Fig. 9).

Morphology and function of motoneuronal subtypes in larval *X. laevis*

The heterogeneity of abducens motoneurons with respect to cell morphology, spontaneous discharge rate, sensitivity, and dynamics of vestibular-evoked responses complies with previous assumptions that the VOR circuitry is arranged in parallel signaling channels, each optimized to a particular range of head motion dynamics (Straka et al., 2009). First evidence was provided by the presence of abducens motor units with markedly different time constants during optokinetic stimulation in adult frogs, suitable for either low-dynamic eye motion or rapid eye movements, respectively (Dieringer and Precht, 1986). The inverse correlation between somal diameter and input resistance and hence excitability (Mendell, 2005) suggests that the spectrum of abducens motoneuronal sizes correlates with a task separation during eye movements (Evinger and Baker, 1991). Moreover, the observed morphological differences might directly match the continuum of resting activities as well as differences in spike amplitude during extracellular multiunit recordings (Lambert et al., 2008).

Different morpho-physiological characteristics of abducens motoneurons comply with a task-specific extraocular motor activity (Evinger and Baker, 1991) and a differential origin of presynaptic inputs from distinct eye movement control areas (Ugolini et al., 2006). A dual organization with respect to response dynamics is implemented for vestibular afferents and central neurons in amphibians (Beraneck et al., 2007; Pfanzelt et al., 2008; Rössert et al., 2011; Gensberger et al., 2015) and other vertebrates (Goldberg, 2000; Straka et al., 2005). Whether this

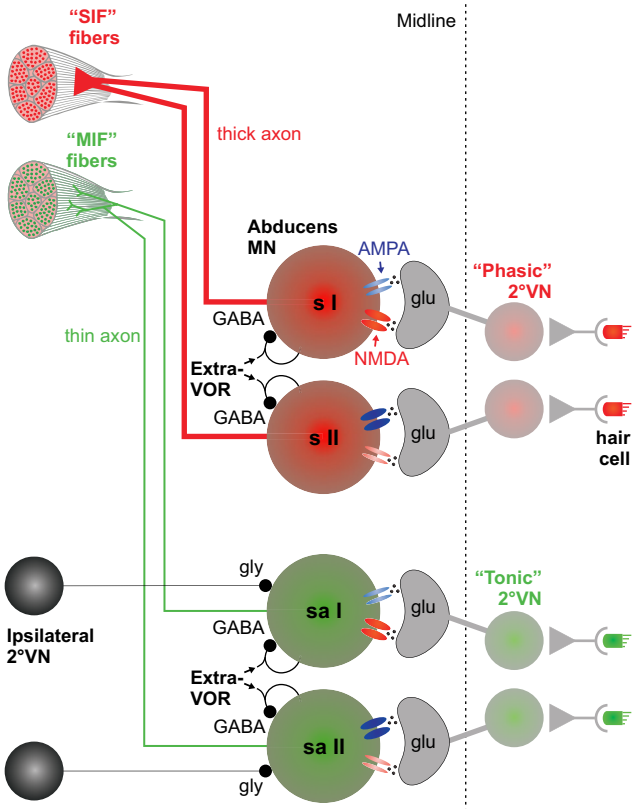

Figure 9. Schematic summarizing the actual and putative anatomical and pharmacological features of *X. laevis* abducens motoneurons. Spontaneously active (sa) or silent (s) abducens motoneurons (MN) distinguish into two subgroups according to differences in response magnitude and timing. AMPA and NMDA response components are inversely correlated in Group I and II motoneurons, respectively. The vestibular excitation of Group I motoneurons consists of a smaller AMPA (light blue) and larger NMDA (dark red) receptor contribution, whereas in Group II motoneurons, the AMPA component (dark blue) considerably surmounts the NMDA (light red) receptor contribution. All motoneurons receive a tonic GABAergic input, whereas the modulated glycinergic ipsilateral vestibular inhibition is discernable only in spontaneously active motoneurons. Based on previous studies (Straka et al., 2009), it appears likely that silent and spontaneously active motoneurons receive excitatory inputs from phasic and tonic 2° vestibular neurons (VN) respectively and mediate these signals separately onto singly (SIF) and multiply innervated (MIF) extraocular muscle fibers. sa I and II, spontaneously active Group I and II abducens motoneurons; s I and II, silent Group I and II abducens motoneurons.

concept of duality is directly transferable to abducens motoneurons is still unclear, but it is compatible with a categorization for example into silent versus spontaneously active motoneurons, although the lesser degree of distinction between these units is rather comparable to the large continuum of resting rates and activation thresholds reported for cat abducens motoneurons (Davis-López de Carrizosa et al., 2011). In addition, the classification of abducens motoneurons into two groups in the current study potentially reflects a functional duality because Group I and II motoneurons show responses during head motion that are reminiscent of the two types of vestibular afferents in larval *X. laevis* (Gensberger et al., 2015). This similarity is compatible with a VOR organization as parallel channels from the sensory periphery to the motor plant.

Despite the lesser degree of separation of Group I and II extraocular motoneurons in *X. laevis* compared with their tonic and phasic presynaptic vestibular neurons (Straka et al., 2005), the two motoneuronal subgroups encode different aspects of head movements. Although neurons in both subgroups are similarly sensitive to increasing stimulus velocities, only responses of Group II motoneurons remain in phase with stimulus velocity, largely independently of stimulus frequency. This suggests that these motoneurons encode the velocity of head motion selectively, its precision being facilitated by the predominance of rapid AMPA receptor-mediated excitatory components (Fig. 6). In contrast, Group I motoneurons respond differentially with respect to amplitude and timing to changes in frequency, possibly by integration of the head acceleration component that changes during varying frequencies. Such an integration might be supported by temporally extended responses resulting from NMDA receptor activation (Fig. 6). The apparent absence of a position sensitivity of abducens motoneurons during sinusoidal rotation complies with the acceleration and/or velocity-related inputs mediated by HC afferents (Holstein et al., 2004), assuming a transfer of these signals to abducens motoneurons by the direct VOR pathway. Because amphibians lack spontaneous saccadic eye movements separated by periods of stable positions (Straka and Dieringer, 2004), at variance with most mammalian species (Stahl and Thumser, 2012), position sensitivity might be less relevant when generating extraocular motor commands in these vertebrates.

A likely motoneuronal task sharing is suggested by data from the modeling approach (Fig. 8) because dynamically appropriate compensatory eye movements during head motion require a combined activation of both motoneuronal groups. In general, Group II motoneurons appear to be more important for VOR-related eye movements (Fig. 8*E*), but predominantly at lower frequencies. In contrast, Group I motoneurons contribute weakly at lower stimulus frequencies, but become increasingly more important at higher frequencies. Whereas spontaneously active units appear to play a larger role for VOR-driven eye motion, silent extraocular motoneurons with large spike amplitudes might trigger high-velocity VOR responses, saccades, or eye twitches (Dieringer and Precht, 1986; Büttner-Ennever and Horn, 2002). Furthermore, the extreme ends of the continuum of silent to spontaneously active motoneurons comply with a general concept where singly and multiply innervated muscle fibers are activated by "twitch-like" (i.e., high-dynamic, silent at rest) and "tonic" (i.e., low-dynamic, spontaneously active) extraocular motoneurons, respectively (Büttner-Ennever and Horn, 2002; Eberhorn et al., 2006).

Organization of excitatory inputs to abducens motoneurons

Glutamatergic inputs from the contralateral vestibular nucleus form the major excitatory drive for abducens motoneurons that, in isolated frog brains, was completely abolished by bath application of the AMPA receptor blocker CNQX (Straka and Dieringer, 1993). Here, excitation of all abducens motoneurons is mediated by a mixture of AMPA and NMDA receptors, compatible with the membraneous presence of both receptor molecules (Durand et al., 1987; Durand, 1991; Keifer and Clark, 2003). The absence of a residual NMDA component after blocking the AMPA component reported previously (Straka and Dieringer, 1993) is likely due to the lack of background resting activity from the vestibular sensory periphery in isolated frog brains. This complies with the spontaneous activity of vestibular afferents in semi-intact tadpole preparations (Gensberger et al., 2015) and the large NMDA sensitivity of abducens motoneuronal resting rates. Moreover, NBQX, which was used in the current study, is more selective for AMPA receptors than CNQX because the latter also partially blocks NMDA receptor-mediated responses (Birch et al., 1988; Long et al., 1990). Therefore, based on the more specific pharmacological intervention in the current study, both glutamate recep-

tor subtypes contribute to the vestibular-driven excitation of abducens motoneurons. Furthermore, the two receptor subtypes independently control the timing of responses during sinusoidal vestibular stimulation because blockade of AMPA receptors causes a phase lag and NMDA receptor inhibition a phase lead in each abducens motor unit. This differential impact is compatible with the short and long time courses of AMPA and NMDA receptor-activated EPSPs, respectively (Edmonds et al., 1995), and complies with the different time courses of AMPA receptor-mediated afferent and NMDA receptor-mediated commissural inputs to central vestibular neurons in frog (Dieringer and Precht, 1977; Straka and Dieringer, 2004). This suggests that AMPA receptors mediate the rapid onset of VOR responses, whereas NMDA receptors encode a longer, sustained activity. These findings comply with a previous pharmacological study (Priesol et al., 2000) demonstrating that AMPA receptor blockade mainly affects the VOR gain during rapid, high-frequency head rotation, whereas NMDA receptor blockade predominantly reduces slow and sustained, low-frequency VOR responses.

Organization of inhibitory inputs to abducens motoneurons

Inhibitory vestibulo-ocular projections onto horizontal and vertical/oblique extraocular motoneurons exhibit different pharmacological profiles (Straka and Dieringer, 2004): glycine is the transmitter for the horizontal and GABA for the vertical VOR (Spencer et al., 1989; Straka and Dieringer, 1993). Nonetheless, rat abducens motoneurons have been shown to possess both glycine and $GABA_A$ receptors, which in slice preparations elicit IPSPs with different time constants (Lahjouji et al., 1996; Russier et al., 2002, Lorenzo et al., 2007). Compatible with these results, all abducens motoneurons in *X. laevis* tadpoles receive a GABAergic and glycinergic inhibition. The more tonic $GABA_A$ receptor-mediated inhibition is unrelated to sinusoidal rotation, hence of nonvestibular origin and potentially mediated by extrasynaptic $GABA_A$ receptors, compatible with a respective location of these receptors in rat abducens motoneurons (Lorenzo et al., 2007). This also complies with the role of $GABA_A$ receptors in regulating neuronal excitability and recruitment threshold of rat oculomotor motoneurons (Torres-Torrelo et al., 2014) and with the robust increase in firing rate after gabazine injections into the abducens nucleus in the current study. The more dendritic location of glycine receptors in rat abducens motoneurons (Lorenzo et al., 2007) is compatible with the rather variable effects of glycinergic inhibition in abducens motoneurons. Nonetheless, the present experiments with isolated inhibitory vestibular inputs suggest that glycine is capable of mediating the inhibitory component of the horizontal angular VOR (Straka and Dieringer, 1993), although it likely predominates in spontaneously active abducens motoneurons, similar to the commissural inhibition of tonic but not phasic frog central vestibular neurons (Malinvaud et al., 2010). Single-cell intracellular characterization of membrane properties and pharmacological profiles will resolve definitively the functional role and efficiency of HC-activated glycinergic inhibition in different types of abducens motoneurons during head rotation.

References

Beraneck M, Pfanzelt S, Vassias I, Rohregger M, Vibert N, Vidal PP, Moore LE, Straka H (2007) Differential intrinsic response dynamics determine synaptic signal processing in frog vestibular neurons. J Neurosci 27:4283–4296. CrossRef Medline

Birch PJ, Grossman CJ, Hayes AG (1988) 6,7-Dinitro-quinoxaline-2,3-dion and 6-nitro,7-cyano-quinoxaline-2,3-dion antagonise responses to NMDA in the rat spinal cord via an action at the strychnine-insensitive glycine receptor. Eur J Pharmacol 156:177–180. CrossRef Medline

Branoner F, Straka H (2015) Semicircular canal-dependent developmental tuning of translational vestibulo-ocular reflexes in *Xenopus laevis.* Dev Neurobiol 75:1051–1067. CrossRef Medline

Broussard DM, DeCharms RC, Lisberger SG (1995) Inputs from the ipsilateral and contralateral vestibular apparatus to behaviorally characterized abducens neurons in rhesus monkeys. J Neurophysiol 74:2445–2459. Medline

Büttner-Ennever JA, Horn AK (2002) Oculomotor system: a dual innervation of the eye muscles from the abducens, trochlear, and oculomotor nuclei. Mov Disord 17:S2–S3. Medline

Büttner-Ennever JA, Horn AK, Scherberger H, D'Ascanio P (2001) Motoneurons of twitch and nontwitch extraocular muscle fibers in the abducens, trochlear, and oculomotor nuclei of monkeys. J Comp Neurol 438:318–335. CrossRef Medline

Carrascal L, Nieto-Gonzalez JL, Torres B, Nunez-Abades P (2009) Changes in somatodendritic morphometry of rat oculomotor nucleus motoneurons during postnatal development. J Comp Neurol 514:189–202. CrossRef Medline

Chagnaud BP, Banchi R, Simmers J, Straka H (2015) Spinal corollary discharge modulates motion sensing during vertebrate locomotion. Nat Commun 6:7982. CrossRef Medline

Davis-López de Carrizosa MA, Morado-Díaz CJ, Miller JM, de la Cruz RR, Pastor AM (2011) Dual encoding of muscle tension and eye position by abducens motoneurons. J Neurosci 31:2271–2279. CrossRef Medline

Dean P (1997) Simulated recruitment of medial rectus motoneurons by abducens internuclear neurons: synaptic specificity vs. intrinsic motoneuron properties. J Neurophysiol 78:1531–1549. Medline

Delgado-Garcia JM, del Pozo F, Baker R (1986) Behavior of neurons in the abducens nucleus of the alert cat. I. Motoneurons. Neuroscience 17:929–952. CrossRef Medline

Dieringer N, Precht W (1977) Modification of synaptic input following unilateral labyrinthectomy. Nature 269:431–433. CrossRef Medline

Dieringer N, Precht W (1986) Functional organization of eye velocity and eye position signals in abducens motoneurons of the frog. J Comp Physiol A 158:179–194. CrossRef

Dietrich H, Straka H (2016) Prolonged vestibular stimulation induces homeostatic plasticity of the vestibulo-ocular reflex in larval *Xenopus laevis.* Eur J Neurosci 44:1787–1796. CrossRef Medline

Dietrich H, Glasauer S, Straka H (2014) Vestibulo-ocular reflexes are mediated by functionally distinct subgroups of extraocular motoneurons. Soc Neurosci Abstr 44:247.07.

Durand J (1991) NMDA Actions on rat abducens motoneurons. Eur J Neurosci 3:621–633. CrossRef Medline

Durand J, Engberg I, Tyc-Dumont S (1987) L-glutamate and N-methyl-D-asparatate actions on membrane potential and conductance of cat abducens motoneurones. Neurosci Lett 79:295–300. CrossRef Medline

Eberhorn AC, Ardeleanu P, Büttner-Ennever JA, Horn AK (2005) Histochemical differences between motoneurons supplying multiply and singly innervated extraocular muscle fibers. J Comp Neurol 491:352–366. CrossRef Medline

Eberhorn AC, Büttner-Ennever JA, Horn AK (2006) Identification of motoneurons supplying multiply- or singly-innervated extraocular muscle fibers in the rat. Neuroscience 137:891–903. CrossRef Medline

Edmonds B, Gibb AJ, Colquhoun D (1995) Mechanisms of activation of glutamate receptors and the time course of excitatory synaptic currents. Annu Rev Physiol 57:495–519. Medline

Evinger C, Baker R (1991) Are there subdivisions of extraocular motoneuronal pools that can be controlled separately? In: Motor control: concepts and issues (Humphrey DR, Freund HJ, eds), pp 23–31. Chichester, UK: Wiley.

Gensberger KD, Gravot C, Hoffman LF, Paulin M, Straka H (2015) Dynamic diversity of horizontal canal afferent neurons in *Xenopus laevis* tadpoles. Soc Neurosci Abstr 45: 235.07.

Gensberger KD, Kaufmann AK, Dietrich H, Branoner F, Banchi R, Chagnaud BP, Straka H (2016) Galvanic vestibular stimulation: cellular substrates and response patterns of neurons in the vestibulo-ocular network. J Neurosci 36:9097–9110. CrossRef Medline

Goldberg JM (2000) Afferent diversity and the organization of central vestibular pathways. Exp Brain Res 130:277–297. CrossRef Medline

Hänzi S, Straka H (2017) Developmental changes in head movement kine-

matics during swimming in *Xenopus laevis* tadpoles. J Exp Biol 220:227–236. CrossRef Medline

Hänzi S, Banchi R, Straka H, Chagnaud BP (2015) Locomotor corollary activation of trigeminal motoneurons: coupling of discrete motor behaviors. J Exp Biol 218:1748–1758. CrossRef Medline

Holstein GR, Rabbitt RD, Martinelli GP, Friedrich VL Jr, Boyle RD, Highstein SM (2004) Convergence of excitatory and inhibitory hair cell transmitters shapes vestibular afferent responses. Proc Natl Acad Sci U S A 101: 15766–15771. CrossRef Medline

Holt GR, Softky WR, Koch C, Douglas RJ (1996) Comparison of discharge variability in vitro and in vivo in cat visual cortex neurons. J Neurophysiol 75:1806–1814. Medline

Horn AK, Leigh RJ (2011) The anatomy and physiology of the ocular motor system. Handb Clin Neurol 102:21–69. CrossRef Medline

Jamali M, Carriot J, Chacron MJ, Cullen KE (2013) Strong correlations between sensitivity and variability give rise to constant discrimination thresholds across the otolith afferent population. J Neurosci 33:11302–11313. CrossRef Medline

Keifer J, Clark TG (2003) Abducens conditioning in in vitro turtle brain stem without cerebellum requires NMDA receptors and involves upregulation of GluR4-containing AMPA receptors. Exp Brain Res 151:405–410. CrossRef Medline

Lahjouji F, Barbe A, Chazal G, Bras H (1996) Evidence for colocalization of GABA and glycine in afferents to retrogradely labelled rat abducens motoneurones. Neurosci Lett 206:161–164. CrossRef Medline

Lambert FM, Beck JC, Baker R, Straka H (2008) Semicircular canal size determines the developmental onset of angular vestibuloocular reflexes in larval *Xenopus.* J Neurosci 28:8086–8095. CrossRef Medline

Lambert FM, Combes D, Simmers J, Straka H (2012) Gaze stabilization by efference copy signaling without sensory feedback during vertebrate locomotion. Curr Biol 22:1649–1658. CrossRef Medline

Long SK, Smith DA, Siarey RJ, Evans RH (1990) Effect of 6-cyano-2,3-dihydroxy-7-nitro-quinoxaline (CNQX) on dorsal root-, NMDA-, kainate- and quisqualate-mediated depolarization of rat motoneurones in vitro. Br J Pharmacol 100:850–854. CrossRef Medline

Lorenzo LE, Russier M, Barbe A, Fritschy JM, Bras H (2007) Differential organization of gamma-aminobutyric acid type A and glycine receptors in the somatic and dendritic compartments of rat abducens motoneurons. J Comp Neurol 504:112–126. CrossRef Medline

Malinvaud D, Vassias I, Reichenberger I, Rössert C, Straka H (2010) Functional organization of vestibular commissural connections in frog. J Neurosci 30:3310–3325. CrossRef Medline

Mendell LM (2005) The size principle: a rule describing the recruitment of motoneurons. J Neurophysiol 93:3024–3026. CrossRef Medline

Nieto-Gonzalez JL, Carrascal L, Nunez-Abades P, Torres B (2007) Phasic and tonic firing properties in rat oculomotor nucleus motoneurons, studied in vitro. Eur J Neurosci 25:2682–2696. CrossRef Medline

Nieuwkoop PD, Faber J (1994) Normal table of *Xenopus laevis* (Daudin): a systematical and chronological survey of the development from the fertilized egg till the end of metamorphosis. New York: Garland.

Pastor AM, Gonzalez-Forero D (2003) Recruitment order of cat abducens motoneurons and internuclear neurons. J Neurophysiol 90:2240–2252. CrossRef Medline

Pastor AM, Torres B, Delgado-Garcia JM, Baker R (1991) Discharge characteristics of medial rectus and abducens motoneurons in the goldfish. J Neurophysiol 66:2125–2140. Medline

Pfanzelt S, Rössert C, Rohregger M, Glasauer S, Moore LE, Straka H (2008) Differential dynamic processing of afferent signals in frog tonic and phasic second-order vestibular neurons. J Neurosci 28:10349–10362. CrossRef Medline

Precht W (1978) Neuronal operations in the vestibular system: studies of brain function. Berlin–Heidelberg: Springer.

Priesol AJ, Jones GE, Tomlinson RD, Broussard DM (2000) Frequency-dependent effects of glutamate antagonists on the vestibulo-ocular reflex of the cat. Brain Res 857:252–264. CrossRef Medline

Ramlochansingh C, Branoner F, Chagnaud BP, Straka H (2014) Efficacy of tricaine methanesulfonate (MS-222) as an anesthetic agent for blocking sensory-motor responses in *Xenopus laevis* tadpoles. PLoS One 9:e101606. CrossRef Medline

Rössert C, Moore LE, Straka H, Glasauer S (2011) Cellular and network contributions to vestibular signal processing: impact of ion conductances, synaptic inhibition, and noise. J Neurosci 31:8359–8372. CrossRef Medline

Russier M, Kopysova IL, Ankri N, Ferrand N, Debanne D (2002) GABA and glycine co-release optimizes functional inhibition in rat brainstem motoneurons in vitro. J Physiol 541:123–137. CrossRef Medline

Schindelin J, Arganda-Carreras I, Frise E, Kaynig V, Longair M, Pietzsch T, Preibisch S, Rueden C, Saalfeld S, Schmid B, Tinevez JY, White DJ, Hartenstein V, Eliceiri K, Tomancak P, Cardona A (2012) Fiji: an open source platform for biological image analysis. Nat Methods 9:676–682. CrossRef Medline

Schuller JM, Knorr AG, Glasauer S, Straka H (2014) Task-specific activation of extraocular motoneurons in *Xenopus laevis.* Soc Neurosci Abstr 44:247.06.

Spencer RF, Wenthold RJ, Baker R (1989) Evidence for glycine as an inhibitory neurotransmitter of vestibular, reticular, and prepositus hypoglossi neurons that project to the cat abducens nucleus. J Neurosci 9:2718–2736. Medline

Stahl JS, Thumser ZC (2012) Dynamics of abducens nucleus neurons in the awake mouse. J Neurophysiol 108:2509–2523. CrossRef Medline

Sterling P (1977) Anatomy and physiology of goldfish oculomotor system. I. Structure of abducens nucleus. J Neurophysiol 40:557–572. Medline

Straka H, Dieringer N (1993) Electrophysiological and pharmacological characterization of vestibular inputs to identified frog abducens motoneurons and internuclear neurons in vitro. Eur J Neurosci 5:251–260. CrossRef Medline

Straka H, Dieringer N (2004) Basic organization principles of the VOR: Lessons from frogs. Prog Neurobiol 73:259–309. CrossRef Medline

Straka H, Simmers J (2012) *Xenopus laevis*: an ideal experimental model for studying the developmental dynamics of neural assembly and sensory motor computations. Dev Neurobiol 72:649–663. CrossRef Medline

Straka H, Gilland E, Baker R (1998) Rhombomeric organization of brainstem motor neurons in larval frogs. Biol Bull 195:220–222. CrossRef Medline

Straka H, Baker R, Gilland E (2001) Rhombomeric organization of vestibular pathways in larval frogs. J Comp Neurol 437:42–55. CrossRef Medline

Straka H, Vibert N, Vidal PP, Moore LE, Dutia MB (2005) Intrinsic membrane properties of vertebrate vestibular neurons: Function, development and plasticity. Prog Neurobiol 76:349–392. CrossRef Medline

Straka H, Baker R, Gilland E (2006) Preservation of segmental hindbrain organization in adult frogs. J Comp Neurol 494:228–245. CrossRef Medline

Straka H, Lambert FM, Pfanzelt S, Beraneck M (2009) Vestibulo-ocular signal transformation in frequency-tuned channels. Ann N Y Acad Sci 1164: 37–44. CrossRef Medline

Torres-Torrelo J, Torres B, Carrascal L (2014) Modulation of the input-output function by GABAA receptor-mediated currents in rat oculomotor nucleus motoneurons. J Physiol 592:5047–5064. CrossRef Medline

Ugolini G, Klam F, Doldan Dans M, Dubayle D, Brandi AM, Büttner-Ennever J, Graf W (2006) Horizontal eye movement networks in primates as revealed by retrograde transneuronal transfer of rabies virus: differences in monosynaptic input to "slow" and "fast" abducens motoneurons. J Comp Neurol 498:762–785. CrossRef Medline